Electromechanical wave imaging (EWI) validation in all four cardiac chambers with 3D electroanatomic mapping in canines *in vivo*

Electromechanical wave imaging (EWI) validation in all four cardiac chambers with 3D electroanatomic mapping in canines *in vivo*

Alexandre Costet[1]**, Elaine Wan**[2]**, Ethan Bunting**[1]**, Julien Grondin**[1]**, Hasan Garan**[2] **and Elisa Konofagou**[1,3,4]

[1] Department of Biomedical Engineering, Columbia University, New York, NY, USA
[2] Department of Medicine—Division of Cardiology, College of Physicians and Surgeons, Columbia University, New York, NY, USA
[3] Department of Radiology, Columbia University, New York, NY, USA

E-mail: ek2191@columbia.edu

Abstract

Characterization and mapping of arrhythmias is currently performed through invasive insertion and manipulation of cardiac catheters. Electromechanical wave imaging (EWI) is a non-invasive ultrasound-based imaging technique, which tracks the electromechanical activation that immediately follows electrical activation. Electrical and electromechanical activations were previously found to be linearly correlated in the left ventricle, but the relationship has not yet been investigated in the three other chambers of the heart. The objective of this study was to investigate the relationship between electrical and electromechanical activations and validate EWI in all four chambers of the heart with conventional 3D electroanatomical mapping. Six ($n = 6$) normal adult canines were used in this study. The electrical activation sequence was mapped in all four chambers of the heart, both endocardially and epicardially using the St Jude's EnSite 3D mapping system (St. Jude Medical, Secaucus, NJ). EWI acquisitions were performed in all four chambers during normal sinus rhythm, and during pacing in the left ventricle. Isochrones of the electromechanical activation were generated from standard echocardiographic imaging views. Electrical and electromechanical activation maps were co-registered and compared, and electrical and electromechanical activation times were plotted against each other and linear regression was

[4] Address to whom any correspondence should be addressed.
1210 Amsterdam Ave., ET351, MC 8904, New York, NY, 10027.

performed for each pair of activation maps. Electromechanical and electrical activations were found to be directly correlated with slopes of the correlation ranging from 0.77 to 1.83, electromechanical delays between 9 and 58 ms and R^2 values from 0.71 to 0.92. The linear correlation between electrical and electromechanical activations and the agreement between the activation maps indicate that the electromechanical activation follows the pattern of propagation of the electrical activation. This suggests that EWI may be used as a novel non-invasive method to accurately characterize and localize sources of arrhythmias.

(Some figures may appear in colour only in the online journal)

Introduction

Arrhythmias such as atrial and ventricular tachycardia, atrial flutter, and atrial fibrillation affect millions of people worldwide (Mozaffarian *et al* 2015). These arrhythmias are the result of abnormal electrical activation patterns in the myocardium, which can result in inefficient contraction of the cardiac muscle leading to poor blood delivery to the rest of body (Fuster *et al* 2007). Initial diagnosis relies on the electrocardiogram (ECG), which provides physicians with a global overview of the electrical activation pattern. The ECG is, however, limited in its characterization of such diseases because it often fails to provide details on the source of the arrhythmia such as the accurate location of the trigger (Yamane *et al* 2001). Electrical mapping via catheterization, usually with fluoroscopic guidance, can be used to further characterize arrhythmias. With mapping, the origin can be detected and radio-frequency (RF) ablation can then be performed on the source in order to terminate the arrhythmia (Lesh *et al* 1994, Hatala *et al* 1996). 3D electroanatomical mapping such as the EnSite (Richmond *et al* 2008) (St. Jude Medical, Secaucus, NJ) or CARTO (Stevenson *et al* 1998) (Biosense-Webster, Diamond Bar, CA) use either electrical or magnetic fields to triangulate the position of the electrodes on the catheter with CT or MRI images in order to reconstruct a 3D shell of the heart chamber which is overlaid with information acquired from catheters in the heart such as electrical activation or voltage map for scar identification (Stevenson *et al* 1998, Tanner *et al* 2010, Szegedi *et al* 2015).

Electromechanical wave imaging (EWI) is a non-invasive, non-ionizing, ultrasound-based imaging modality that can map the electromechanical activity of the heart in all four chambers at high spatial and temporal resolution, with real-time feedback capabilities for imaging at the point of care (Provost *et al* 2010, 2011b, 2011c, 2012, 2013, Costet *et al* 2014). The electromechanical activity of the heart refers to the onset of the mechanical activity that is triggered by the propagation of the electrical activation, i.e. the first time at which the muscle transition from a relaxation to a contraction state after depolarization. The short delay between the depolarization and the activation of the muscle fibers is called the electromechanical delay and its value has been reported being between 20 and 40 ms (Bers 2002, Cordeiro *et al* 2004). The electromechanical wave (EW) denotes the spatial propagation along the cardiac muscle of the electromechanical activation that follows the electrical activation. EWI relies on speckle-tracking techniques on ultrasound RF frames in order to estimate minute displacements and incremental (or inter-frame) strains, i.e. the change in cumulative strain between consecutive

frames. A sufficient high frame rate enables the detection of the very onset of deformation within the heart that we previously defined as EW (Provost *et al* 2012).

EWI was previously shown to be capable of mapping the electromechanical activation sequence epicardially, endocardially and across the myocardium in both human (Provost *et al* 2011b, 2013, 2015) and canine (Provost *et al* 2010, 2011b, 2011c, 2012, Costet *et al* 2014, 2015) models, during sinus rhythm, focal pacing, and arrhythmias both of re-entrant or focal origin. EWI was also shown to be capable of localizing the site of pacing, both for conventional pacing and biological pacing (Provost *et al* 2013, Costet *et al* 2014). Previous studies found that the electromechanical activation, i.e. the EW, and the electrical activation followed a similar pattern of propagation in the left ventricle (LV). Indeed, the EW was directly correlated with the underlying electrical activation in the LV of normal canine hearts during sinus rhythm and various pacing protocols *in vivo* and *in silico* (Provost *et al* 2011b, 2011c). These results suggest that the electrical activation and the electromechanical activation, as depicted by EWI, follow the same pattern of activation in the heart. However, the relationship between the electrical and electromechanical activation has not yet been investigated in the other three chambers of the heart: the left atrium (LA), the right atrium (RA), and the right ventricle (RV). Since atrial arrhythmias such as atrial tachycardia, atrial flutter and fibrillation occur in both the LA and RA while ventricular tachycardia can originate from the RV, a large number of arrhythmias do not occur in the LV and the relationship between the electromechanical and electrical activations needs to be investigated in all four chambers of the heart with EWI.

In this study, we investigate the relationship between the electrical and electromechanical activations in all four chambers of the heart. In order to facilitate co-registration between electrical and electromechanical maps, we use a 3D electroanatomical mapping system (EnSite, St. Jude Medical, Secaucus, NJ) to obtain 3D electrical activation maps. At the same time, EWI provides pseudo-3D maps of the electromechanical activation. Both types of activation maps are then co-registered and compared qualitatively and quantitatively. Linear correlation between electrical and electromechanical activations is found in all cases, demonstrating that the EW follows the same pattern of propagation as the electrical activation in all four chambers of the heart.

Methods

Experimental protocol

This study complied with the Public Health Service Policy on Humane Care and Use of Laboratory Animals and was approved by the Institutional Animal Care and Use Committee of Columbia University. Six ($N = 6$) male adult mongrel canines (weight $= 24.4 \pm 0.9$ kg) were used in this study. After opening the chest by lateral thoracotomy, a pericardial cradle was formed to exclude the lungs and support the heart in order to expose the apex. In this study, both epicardial and endocardial electrical mappings were performed in order to validate EWI on both surfaces of the heart. Two types of catheters were used in this study: a bipolar catheter (TactiCath, St. Jude Medical, Secaucus, NJ) and a 64-electrode basket catheter (Constellation, Boston Scientific, Natick, MA). The type of catheter chosen for mapping was chosen depending on the surface of mapping as well as availability. The basket catheter allows for simultaneous acquisition of 56 signals in the endocardium (i.e. 64 electrodes providing 56 pairs of electrodes for bipolar acquisition), whereas a bipolar catheter may only acquire one signal per heart cycle. Bipolar catheters, however, are better suited for epicardial mapping since the catheter tip can be dragged over the heart during acquisition. The 64-electrode basket catheter was introduced in the LV in one canine ($n = 1$), and in the right atrium (RA) in one

other canine ($n = 1$) to acquire endocardial electrical activation data with the St. Jude EnSite electroanatomical mapping system (St. Jude Medical, Secaucus, NJ). The bipolar catheter was used in the other four ($n = 4$) canines to acquire both epicardial electrical activation data (in three canines) and endocardial electrical activation data (in one canine). Note that endocardial mapping with the bipolar catheter was performed in the right ventricle (RV) by inserting the catheter in the chamber and recording data with the EnSite system as the tip of the catheter was positioned at different locations on the septum.

Electromechanical wave imaging

EWI was acquired during sinus rhythm and pacing at a cycle length 400 ms on open-chest canines in the standard apical echocardiographic views (4-chamber, 2-chamber, and 3-chamber) with an additional view acquired in between the 2- and 4-chamber views that we call '3.5-chamber' view (figure 1). The ultrasound probe, coated with ultrasound gel, was positioned directly on the heart at the apex. An unfocused transmit sequence was used on a Verasonics system (Verasonics, Redmond, WA) in order to acquire ultrasound RF frames at 2000 fps using a 2.5 MHz ATL P4-2 phased array. Such a high frame rate can be achieved by emitting unfocused circular ultrasound waves using a virtual focus located 10.2 mm behind the array (figure 2(1)) (Provost *et al* 2011c). Owing to the fact that the B-mode images reconstructed from these unfocused transmit sequences have lower resolution and signal-to-noise ratio (SNR) thus rendering segmentation difficult, a standard 64-line B-mode acquisition was performed following the initial high frame rate acquisition. The complete acquisition sequence consisted of 2 s of high frame rate acquisition at 2000 fps (4000 frames acquired), followed by an anatomical imaging sequence consisting of 1.5 s of a standard 64-line B-mode acquisition at 30 fps. Retrospective ECG-gating was used in order to temporally align the high frame rate acquisition with the anatomical B-mode acquisition (figure 2(1)). Beamforming on the element data obtained from each of the elements was performed during post-processing, resulting in the reconstruction of one RF frame per transmit. RF frames denote the beamformed, unprocessed and unfiltered ultrasound images that contain phase information that is lost when generating B-mode images. Ultrasound RF frames were reconstructed in polar coordinates from the raw signals obtained from the probe elements using a delay-and-sum algorithm. The reconstructed images had an angular sampling of 0.7° or 0.025 rad (128 lines spanning 90°) and an axial sampling frequency of 20 MHz (axial sampling of 0.0385 mm) (figure 2(2)). Segmentation of the myocardium was manually performed on the first frame of the anatomical B-mode sequence and the endocardial contour was subsequently automatically tracked throughout the cardiac cycle using the estimated displacements (Luo and Konofagou 2008). Displacement estimation was performed using a fast, 1D RF-based cross-correlation algorithm with overlapping 6.2 mm axial windows (10 wavelengths) and a 0.62 mm window shift (90% overlap) (Luo and Konofagou 2010) (figure 2(3)). RF-based speckle tracking techniques have be shown to offer far greater accuracy than B-mode speckle tracking techniques (Walker and Trahey 1994). Axial incremental strains (i.e. the inter-frame strain in the axial direction) were estimated using a least-squares estimator with a 5 mm, 1D-kernel (Kallel and Ophir 1997). Strain estimates were then filtered using a 12 mm by 10 beams moving average spatial filter and a temporal low-pass filter with a 125 Hz cut-off frequency (figure 2(4)). The displacement and strain estimations were both performed in polar coordinates. Displacements and strains were subsequently converted to Cartesian coordinates. The incremental strain, or inter-frame strain, corresponds to the change in cumulative strain between two consecutive frames. Indeed, the incremental strain and the cumulative strain are linked through a temporal
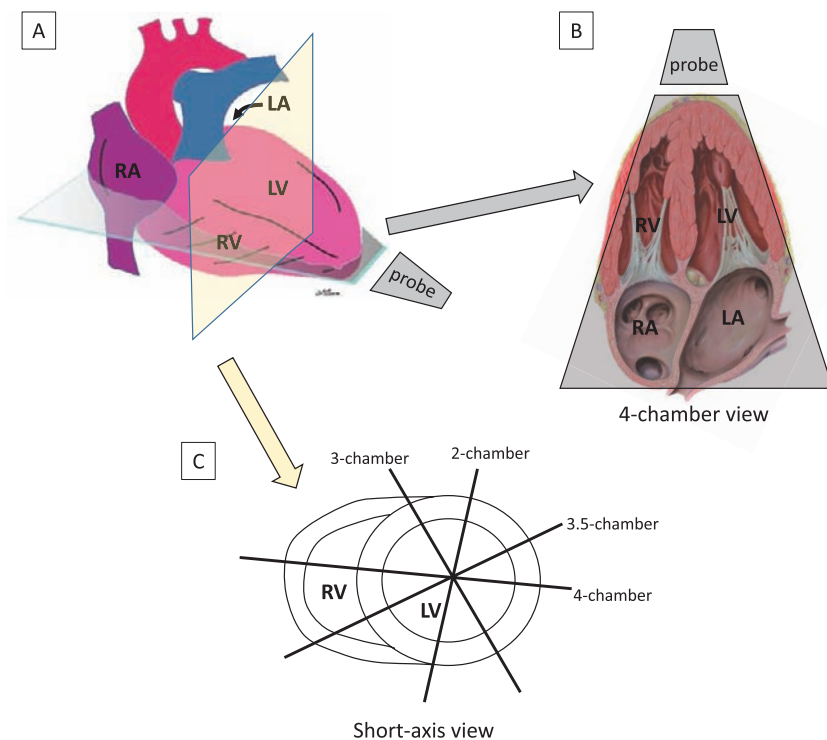
Figure 1. Echocardiographic views. (A) Position of the probe when acquiring a 4-chamber view (grey). The yellow plane represents the short-axis plane of view. (B) Apical 4-chamber view superimposed on a diagram of the heart. (C) Short axis views detailing all four EWI apical views used in this study. LA/RA = left/right atrium, LV/RV = left/right ventricle. Heart diagram in (A) courtesy of www.echocardiographer.org.

derivative, which means that when the cumulative strain reaches a maximum or minimum, the incremental strain will be equal to zero. In other words, when the heart changes its behavior, i.e. from relaxation to contraction and vice versa, the incremental strain crosses zero. The type of zero-crossing (positive-to-negative or negative-to-positive) will depend on the orientation of the wall with respect to the axial direction of estimation. For example, previous studies showed that in the ventricles contraction of the heart results in radial thickening and circumferential and longitudinal shortening (Waldman *et al* 1985, Villarreal *et al* 1991, Lee *et al* 2007, 2011). As a result, the electromechanical activation will be defined in the radial direction as a negative-to-positive zero-crossing (thickening) while it will be defined in the circumferential and longitudinal directions as a positive-to-negative zero-crossing (shortening). Based on this definition of the electromechanical activation, we subsequently generated isochrones by mapping the first occurrence of the incremental strain crossing zero in the ventricles (i.e. onset of contraction) after the onset of the electrical activation whose origin was taken as the beginning of the QRS ($t = 0$ ms). In the atria, the origin was chosen as the P-wave. The zero-crossing timings were semi-manually obtained in a range of 60–100 randomly and automatically selected regions. A sub-sample resolution was obtained through cubic spline interpolation, and smooth continuous isochronal maps were then generated through a Delaunay triangulation-based cubic interpolation. Finally, isochrones for all views were co-registered in Amira 5.3.3 (Visage Imaging, Chelmsford, MA, USA) to generate pseudo-3D isochrones (figure 2(5)).
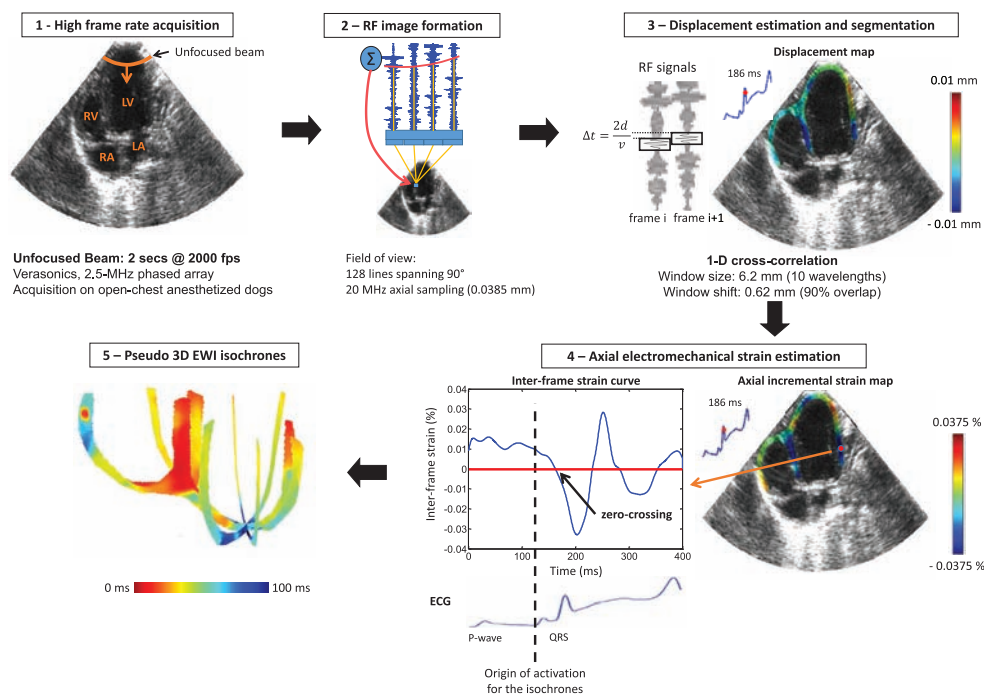
Figure 2. EWI acquisition and motion and strain estimation flowchart. (1) 2 s high frame rate acquisition (2000 Hz) in standard apical views with an unfocused transmit sequence. (2) RF image formation using channel data. (3) Segmentation and 1D axial displacement estimation using 1D cross-correlation. Motion maps are generated. (4) Axial incremental strain estimated using a least-square estimator. (5) EWI isochrones are obtained semi-manually by mapping zero-crossings within the mask for each apical view. Pseudo 3D isochrones are then generated. LA/RA = left/right atrium, LV/RV = left/right ventricle, RF = radio-frequency.

Co-registration was performed both temporally and spatially. Temporal co-registration was achieved by choosing the same origin for each single-view isochrone (the beginning of the QRS on the ECG) and the same color scale for activation time (e.g. $t = 0$ ms to $t = 150$ ms). Spatial co-registration was achieved by using B-mode anatomical landmarks such as the position of the valves and apex to align each view with respect to the others.

Co-registration and comparison between EWI and EnSite activation maps

Figure 3 depicts a block diagram of the methodology employed for co-registering electrical and electromechanical activation maps. Since EWI isochrones could not be imported into the EnSite system, data from the EnSite system was exported to a workstation for co-registration with EWI isochrones. 3D maps of the electrical activation are generated by the EnSite system through interpolation from a finite number of acquired point, each defined by their spatial coordinates and the corresponding activation time. It is not possible to directly export the full 3D mesh from the EnSite system. Only comma-separated-value files containing the coordinates and activation times of the acquired points used for generating the 3D electrical activation maps as well as the coordinate of the vertices and edges of the mesh may be exported. As a result, in order to be able to co-register both the 3D electrical activation maps and the pseudo-3D electromechanical activation maps, the 3D mesh was re-generated in Maya (Maya
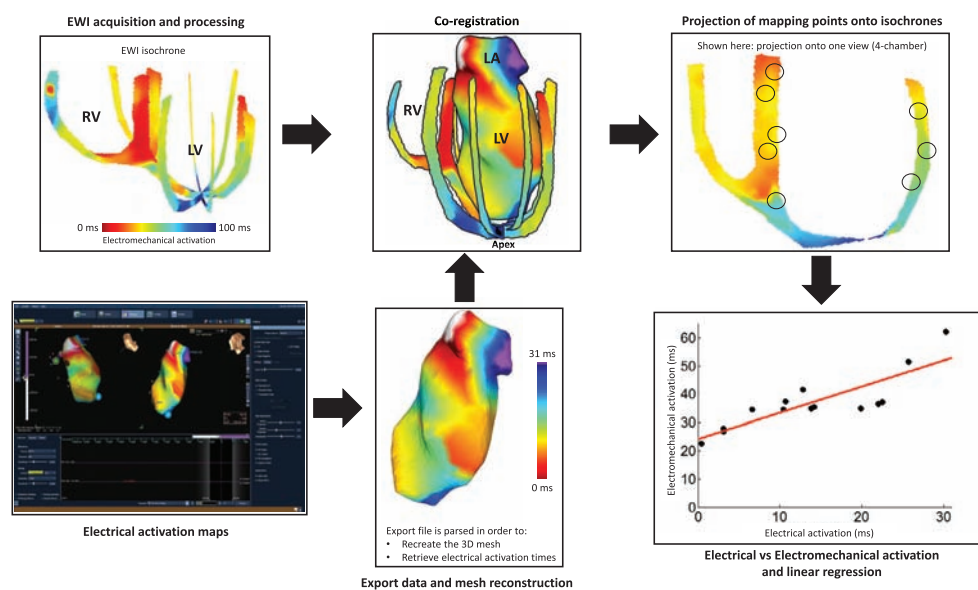
Figure 3. Block diagram of the processing for EWI validation with 3D electroanatomical mapping. Both electromechanical and electrical activation maps are generated and co-registered using anatomical landmarks. Plots of electromechanical versus electrical activation times are then generated and linear regression is performed to obtain slope, intercept and R^2 values.

2016, Autodesk, San Rafael, CA, USA) and the full 3D electrical activation map was then re-generated using the open-source software MeshLab (Visual Computing Lab—ISTI, CNR, meshlab.sourceforge.net). This extra step allowed us to obtain two files in the same format for comparison: one for the electrical activation map and the other for the electromechanical activation map. The 3D co-registration was performed by aligning the pseudo-3D electromechanical isochrones with the 3D electrical maps in Amira using anatomical landmarks such as the location of the apex, the mitral valve annulus, the lateral wall, or the septum, all of which can be marked on the 3D electrical activation maps. Once both the electromechanical activation isochrones and the electrical activation map were aligned, the location of the points acquired with the EnSite system were projected onto the closest EWI isochrone, and activation times were compared. If the location of the point acquired during electrical mapping fell in between two EWI views, the location was projected to the closest points on each view and the average of both EWI activation times was used for comparison. This step provided pairs of electrical and electromechanical activation times, which were then plotted against each other. Linear regression was performed and slope, intercept, R^2 and *p*-values were obtained. The number of point considered for the linear regression corresponds to the number of points acquired during electrical mapping as we did not use the values of interpolated points.

Results

Figures 4–7 depict the 3D electrical activation maps and the pseudo-3D electromechanical activation maps as well as the results of the linear regression between electrical and electro-mechanical activations for the LA, LV, RA, and RV. Linear regression results are also summarized in table 1 for all mapping cases.
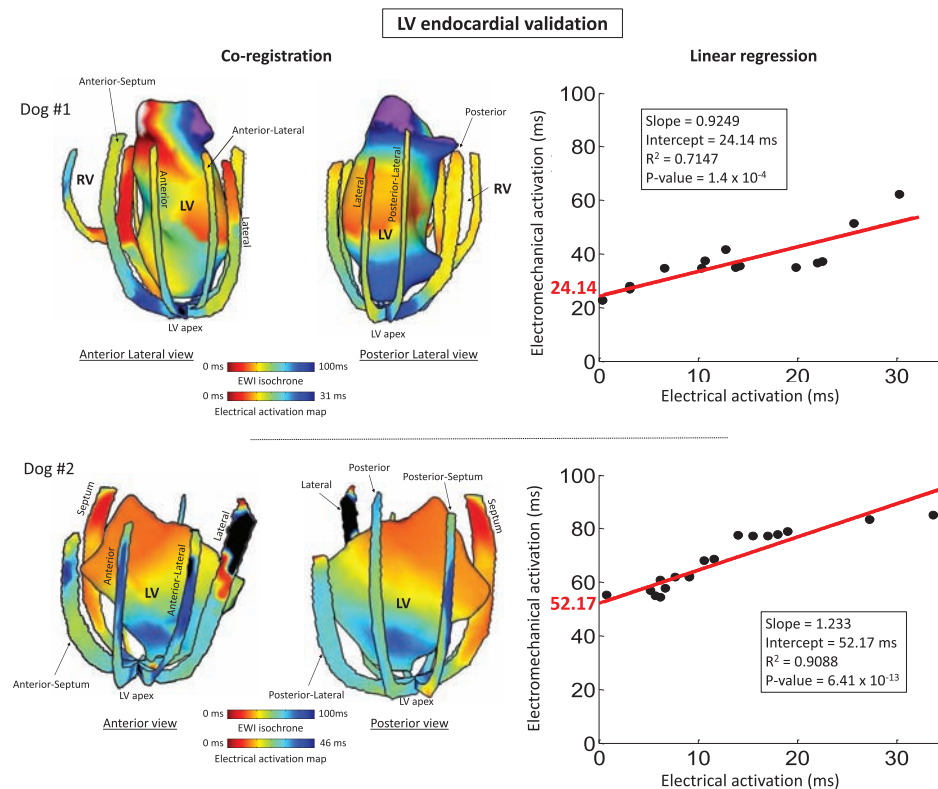
Figure 4. LV endocardial EWI validation in two canines during normal sinus rhythm. Both electrical activation maps were acquired using a 64-electrode basket catheter. The origins of both activation maps ($t = 0$ ms) correspond to the beginning of the QRS on the ECG. LV/RV = left/right ventricle.

Figure 4 depicts endocardial validation in the LV for two different animals. A 64-electrode basket catheter was used in both cases. For each animal, the co-registration between the 3D electrical activation maps and pseudo-3D EWI isochrones is shown on the left. On the right, plots of the electromechanical versus electrical activation are shown as well as the linear regression results. Not all 64 electrodes had good contact with the myocardium, which resulted in some electrodes not recording any electrical signal. As such, only the electrodes for which a signal was recorded were considered. During mapping of the endocardial activation in the LV, a slope of 0.93 with an intercept of 24.15 ms and a R^2 value of 0.71 (p-value = 0.000 14) was found in the first animal, and a slope of 1.23, an intercept of 52.17 ms and a R^2 value of 0.91 (p-value $\ll$ 0.0001) was found in the second animal.

Figure 5 depicts the results for epicardial LV validation during sinus rhythm and pacing in the same animal. Pacing was performed via an external electrode sutured laterally on the LV, near the base. Linear regression yielded a slope of 1.61, a 57.74 ms intercept and a R^2 value of 0.87 (p-value $\ll$ 0.0001) during sinus rhythm, a slope of 1.83, a 58.6 ms intercept and a R^2 value of 0.89 (p-value $\ll$ 0.0001) during pacing.

Figure 6 depicts the result of the validation in the RV. The RV epicardial map was generated from recording sites on the anterior, RV free wall and the parts of the posterior wall that were accessible epicardially. An endocardial electrical activation map was generated by recording sites on the RV septum. The two sets of pairs of electrical and electromechanical activation
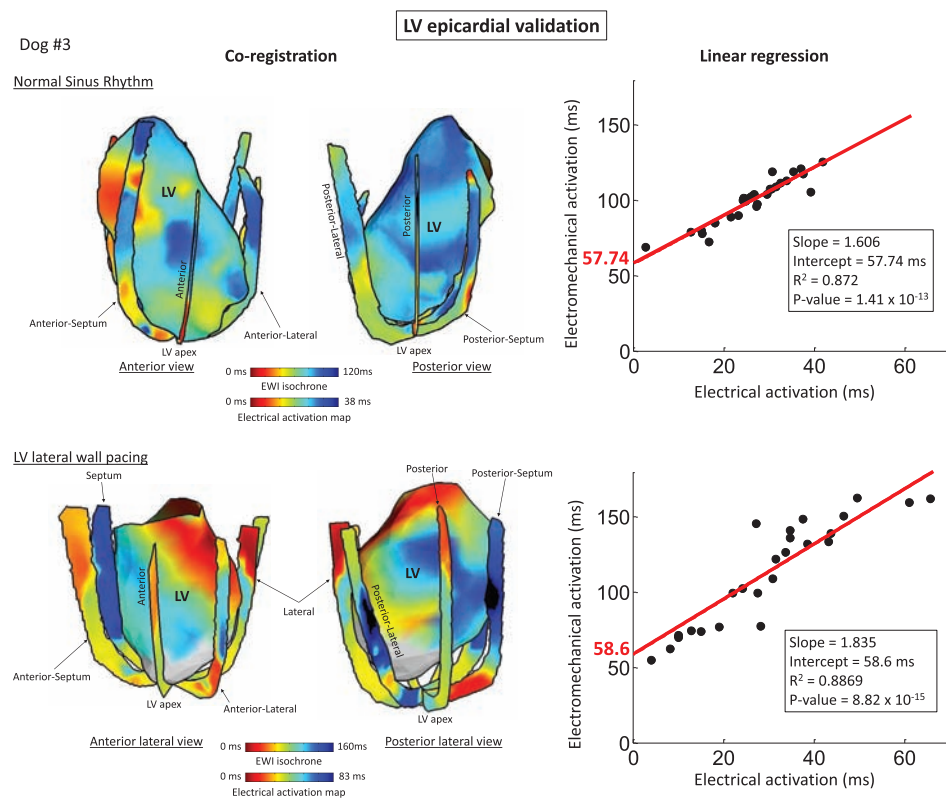
Figure 5. LV epicardial EWI validation in one canine during normal sinus rhythm and during LV lateral wall focal pacing. The electrical activation maps were acquired using a bipolar catheter. The origins of both activation maps ($t = 0$ ms) correspond to the beginning of the QRS on the ECG. LV/RV = left/right ventricle.

times obtained from comparing the endocardial and epicardial maps to the pseudo-3D EWI isochrone were combined into a single set that was used for the linear regression analysis. Results yielded a linear correlation with a slope of 1.29, an intercept of 18.68 ms and a R^2 value of 0.81 (*p*-value $\ll$ 0.0001).

Finally, figure 7 shows validation results in both atria. Figure 7(A) shows endocardial validation in the RA using a 64 electrode basket catheter. Only electrodes that had good contact with the myocardium were considered for the linear regression analysis. Linear regression yielded a slope of 0.77, an intercept of 47.55 ms and a R^2 value of 0.78 (*p*-value = 0.000 16). Figure 7(B) shows epicardial validation in the LA and the anterior/lateral part of the RA (the posterior part of the RA could not be reached with the mapping catheter). The linear regression yielded a slope of 1.10, an intercept of 9.20 ms and a R^2 value of 0.81 (*p*-value $\ll$ 0.0001).

Discussion

In this study, we investigated the relationship between electrical and electromechanical activations in all chambers of the heart and showed for the first time in all four chambers of the heart that the electromechanical and electrical activations were linearly correlated. Previously, EWI validation in the LV was achieved *in silico* using an *in vivo* based canine cardiac
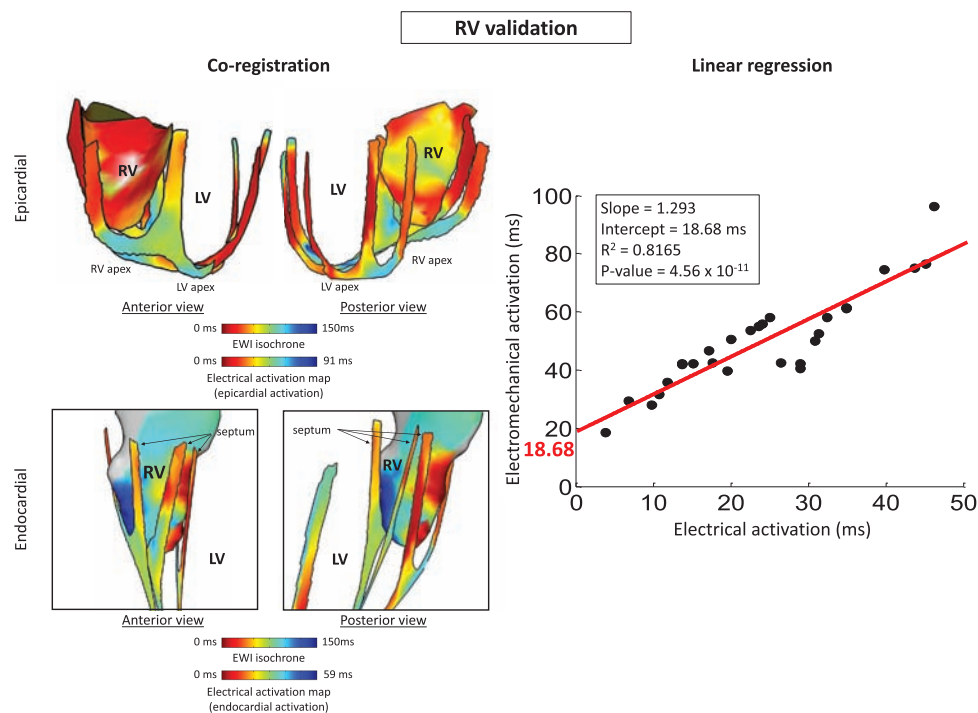
Figure 6. RV EWI validation in one canine during normal sinus rhythm. Epicardial map of the anterior, lateral, and some posterior regions (top) and endocardial activation map of the septum (bottom) were acquired using a bipolar catheter. 4-chamber, 3-chamber, and 5-chamber views were used to generate the pseudo 3D EWI isochrones. Both endocardial and epicardial points are used to generate the linear regression. The origins of both activation maps ($t = 0$ ms) correspond to the beginning of the QRS on the ECG. LV/RV = left/right ventricle.

electromechanics model (Provost *et al* 2011a), and *in vivo* by either suturing a limited number of electrodes onto the heart (Provost *et al* 2011b) or using a 64-electrode basket catheter (Provost *et al* 2011c). Limitations of these methods included the limited number of recording sites in the first case, and in the other case challenging co-registration due to difficulty in accurately determining the positions of the basket catheter electrodes. Additionally, until now, validation had only been performed in the LV. Herein, we found that the electrical activation and the EW followed similar pattern of activation in all four chambers of the heart. Indeed, in line with results from previous studies (Provost *et al* 2011b, 2011c), correlation between the electromechanical and electrical activation was found to be linear with slopes ranging from 0.77 to 1.61 during normal sinus rhythm, and a slope of 1.83 during LV pacing. Previous studies investigating the relationship between electromechanical and electrical activations also reported a linear correlation in the LV between the electromechanical and electrical activations using MRI tagging and an electrode sock during RV pacing, with linear regression slopes ranging from 0.87 to 1.05 (Faris *et al* 2003). Intercepts of the linear regression can be likened to the delay between the electrical and electromechanical activations, otherwise known as the electromechanical delay. The delays were found to range between 9.2 and 58.7 ms and are similar to previously reported values ranging from 20 to 47 ms (Provost *et al* 2011b, 2011c).
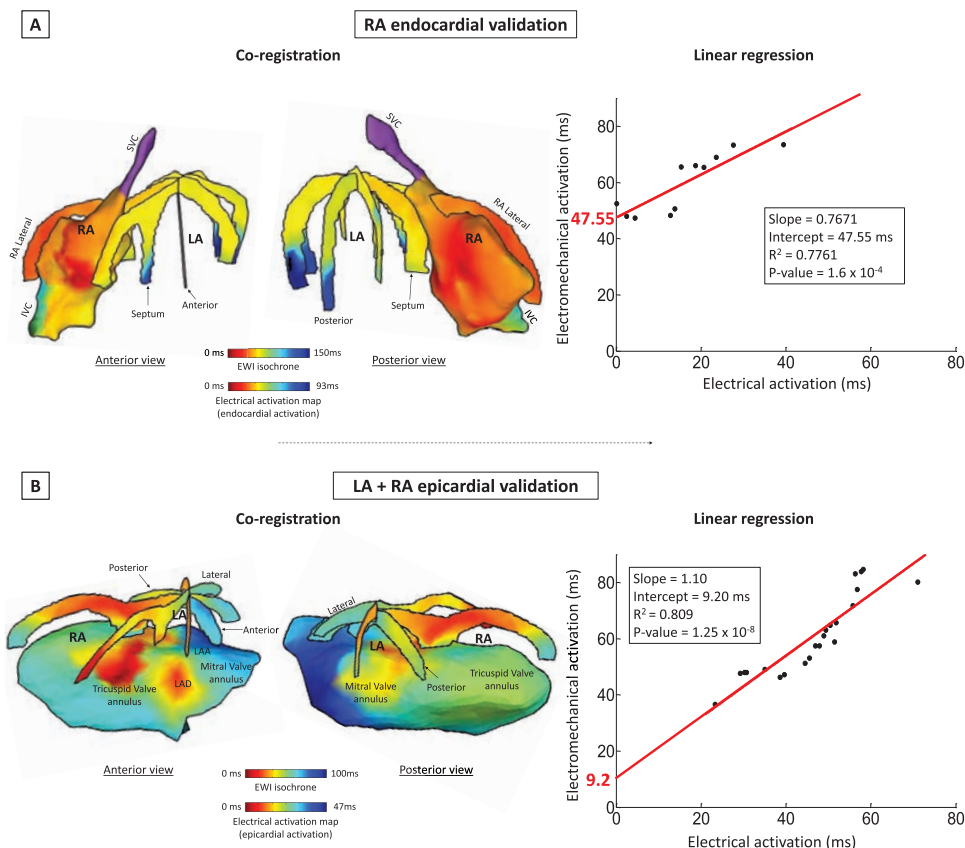
Figure 7. Atrial EWI validation in two canines during normal sinus rhythm. (A) Endocardial RA validation, (B) LA and RA epicardial validation. Both endocardial and epicardial maps were acquired using a bipolar catheter. The origins of both activation maps ($t = 0$ ms) correspond to the beginning of the *P*-wave on the ECG. IVC/SVC = inferior/superior vena cava, LA/RA = left/right atrium, LAD = Left anterior descending artery, LV/RV = left/right ventricle.

A slope of 1 would suggest constant electromechanically delays through the heart, given by the intercept. Although in this study some slopes had values close to unity, this was not always the case. A slope higher than 1 implies a lengthening of the electromechanical delay while a slope lower than 1 implies a shortening of the electromechanical delay. This may be explained by the mechanical component of the electromechanical activation. Indeed, Faris *et al* (2003) found that, in the ventricles, the electromechanical delays in the heart during RV pacing was the shortest at 10–20 ms in regions near the pacing site and increased to 50–90 ms in regions far from the pacing site in the LV. They attributed the increase in the delays to tethering of the tissue during contraction, i.e. the distal sites in the LV had to contract against already contracting tissue in the RV, which might have resulted in delayed tissue shortening. Thus, tethering of the tissue during systole may explain the slope values differing from unity. The anisotropy induced by the varying orientation of the cardiac fibers through the heart, as well as across different hearts, may also be a factor in explaining the different values of the slope of the correlation. However, because all linear regressions had high correlation coefficient, this

Table 1. Summary of the linear regression results for each validation case.

Sinus rhythm						
Animal #	Chamber	Type	Slope	Intercept (ms)	R^2	*P*-value
1	LV	Endo	0.92	24.14	0.71	1.4×10^{-4}
2	LV	Endo	1.23	52.17	0.91	6.41×10^{-13}
3	LV	Epi	1.61	57.74	0.87	1.4×10^{-13}
4	RV	Endo + Epi	1.29	18.68	0.82	4.56×10^{-11}
5	RA	Endo	0.77	47.55	0.78	1.6×10^{-4}
6	LA + RA	Epi	1.10	9.20	0.81	1.15×10^{-8}
LV lateral pacing						
Animal #	Chamber	Type	Slope	Intercept (ms)	R^2	*P*-value
3	LV	Epicardial	1.83	58.60	0.89	8.82×10^{-15}

Abbreviations: Endo = endocardial, Epi = epicardial, LA = Left atrium, LV = left ventricle, RA = right atrium, RV = right ventricle.

suggests that the electromechanical activation follows the same pattern of propagation as the electrical activation.

The current gold standard for characterizing the focal triggers or sources of arrhythmias involves invasive catheterization of the heart and recording sites on the endocardium or epicardium in painstaking detail. 3D electroanatomical mapping systems such as the EnSite and CARTO systems have become ubiquitous for mapping and RF ablation procedures. Limitations of such mapping techniques include sequential acquisition over several heartbeats resulting in long mapping duration, as well as the need for fluoroscopic guidance which requires patient exposure to ionizing radiation. Other non-invasive mapping techniques have been in development and are currently being used in clinical trials. One such technique is electrocardiographic mapping or electrocardiographic imaging (Ramanathan *et al* 2004, Cakulev *et al* 2013) which can recreate epicardial activation maps in a single heartbeat from 256 body surface electrodes. The technique has already been successfully used in the clinic but it requires the patients to undergo a CT scan in order to obtain heart-torso geometry, which exposes the patient to radiation and may be costly.

EWI, is a mobile, non-invasive, ultrasound-based technique that can provide information on the electromechanical activation in the heart. EWI validation in all four chambers of the heart suggests that EWI may have the potential to non-invasively characterize cardiac rhythms in all chambers of the heart in a single acquisition. Indeed, initial feasibility studies showed that EWI could be used to map the electromechanical activation during atrial tachycardia, flutter and fibrillation, as well as in cardiac resynchronization therapy patients with left bundle brunch block (Provost *et al* 2013, 2015, Costet *et al* 2015). Thus, EWI may provide additional information for the study and characterization of arrhythmias in the clinic as a pre-procedural tool for planning invasive mapping and ablation procedures.

Most of the current EWI processing pipeline is automated. Manual inputs include selection of the cardiac cycle to process as well as segmentation of the walls can be performed by an untrained operator in a matter of seconds. Even though it only requires a couple of minutes to complete, the isochrone generation step is still mostly manual and requires some training. In order for EWI to be fully ready for clinical use, automation of the isochrone generation process will need to be implemented. This is currently being investigated in our lab.

Limitations in this study include the low number of animals used for validation as a larger number of animal would have enabled statistical significance testing. Another limit is the fact that the EnSite system was used on open-chest canines instead of humans. Indeed, the EnSite system is designed for clinical use and, as such, is calibrated to the human anatomy. Detection of the position of the electrode in space relies on changes in electric fields generated by the EnSite system through surface electrodes placed on the subject. Although the anatomy of the hearts of canines is very similar to that of human hearts, their overall anatomy is obviously different. As a result, the positioning of the surface electrodes will be suboptimal which may result in some of the 3D meshes not being anatomically correct and may in turn complicate 3D co-registration. Mitigation of this issue relies on a feature of the EnSite system which enables the operator to add labels on the 3D model at the position of the catheter, thus helping with the orientation of the mesh with respect to the isochrones. While open-chest imaging provides excellent acoustic windows for ultrasound imaging, transthoracic EWI on human subjects will introduce attenuation and poor acoustic windows. This did not prove, however, to be a major issue in previous close-chest EWI studies (Provost *et al* 2011b, 2013, 2015, Costet *et al* 2014).

Another limitation of this study lies with the 2D imaging of a 3D propagation. One solution to this problem is to acquire multiple 2D views in order to capture as much of the 3D pattern as possible. Those 2D views can then be used to recreate pseudo-3D isochrones thus enabling sufficient sampling of the 3D propagation pattern. Furthermore, incremental displacement and strain estimation were performed in 1D in the axial direction only. As discussed in the methods section, when the axial direction of estimation is aligned with the longitudinal or radial direction of the wall, the onset of electromechanical activation corresponds to a zero-crossing of the incremental strain. Misalignment of the wall with respect to the axial direction may, however, introduce projection errors and, as a result, may decrease the magnitude of the incremental strain values. Since EWI only concerns itself with the timing of the zero-crossings and not the incremental strain value, this will not be an issue unless the angle of projection is close to 45°. In that case, the magnitude of the incremental strain may be close to or fall below the noise-level and picking a zero-crossing time for that region might not be possible. Because this will only concern a very limited number of regions on the apical echocardiographic views, it should not impact the overall isochrones significantly.

Finally, another limitation could arise from the fact that the electrical and electromechanical activation maps are not simultaneously acquired and thus do not correspond to the same heart cycle. However, this was not a concern of ours because we are mapping and performing EWI on highly organized, stable rhythms (either sinus rhythm or focal pacing), and because we have previously shown EWI to be reproducible and repeatable between heart cycles both within the same acquisition and between separate acquisitions (Provost *et al* 2013, Costet *et al* 2014). Finally, EWI relies on the electromechanical coupling of the myocardium. Some arrhythmias, in particular arrhythmias related to ischemia and infarct, induce a decoupling between the electrical and mechanical components of the heart. In regions of ischemia and infarct, the muscle hardly moves and decorrelation will be expected. Atrial fibrillation may also be difficult to map due to fibrosis and contractile deficiency. However, one could infer that EWI may be useful in detecting hypokinetic and akinetic regions since these regions will present lower strain values. Thus, EWI may potentially non-invasively identify regions of scar and infarct. EWI could also detect regions where the electromechanical coupling is breaking down which may be useful in the prediction of CRT response (Sermesant *et al* 2012, Lumens *et al* 2015). Of course, further study is necessary to investigate such claims.

Conclusion

In this study, we investigated the relationship between electrical and electromechanical activations in all chambers of the heart. EWI was validated with 3D electroanatomical mapping in all four chambers of the heart in a large animal model. 3D electroanatomical mapping allowed for a more accurate co-registration between the electrical and the electromechanical activation maps. Linear correlation was found between electrical and electromechanical activations, which implies that the electromechanical wave follows the pattern of propagation of the electrical activation. This suggests that EWI may be a useful and powerful non-invasive tool to accurately characterize the activation sequence in the heart during normal rhythm and focal rhythms. Clinically, EWI may be used to characterize arrhythmias and pre-procedurally plan invasive mapping and ablation, which may reduce risk to patients by minimizing radiation and prolonged procedure times.

Acknowledgments

References

Bers D M 2002 Cardiac excitation-contraction coupling *Nature* **415** 198–205
Cakulev I *et al* 2013 Confirmation of novel noninvasive high-density electrocardiographic mapping with electrophysiology study implications for therapy *Circ. Arrhythm Electrophysiol.* **6** 68–75
Cordeiro J M, Greene L, Heilmann C, Antzelevitch D and Antzelevitch C 2004 Transmural heterogeneity of calcium activity and mechanical function in the canine left ventricle *Am. J. Physiol. Heart Circ. Physiol.* **286** H1471–9
Costet A, Bunting E, Grondin J, Gambhir A and Konofagou E E 2015 Atrial electromechanical cycle length mapping in paced canine hearts *in vivo IEEE Trans. Ultrason. Ferroelectr. Freq. Control* **62** 1277–87
Costet A *et al* 2014 Electromechanical wave imaging of biologically and electrically paced canine hearts *in vivo Ultrasound Med. Biol.* **40** 177–87
Faris O P *et al* 2003 Novel technique for cardiac electromechanical mapping with magnetic resonance imaging tagging and an epicardial electrode sock *Ann. Biomed. Eng.* **31** 430–40
Fuster V, O'Rourke R, Walsh R and Poole-Wilson P 2007 *Hurst's the Heart* 12th edn (New York: McGraw-Hill)
Hatala R, Weiss C, Koschyk D H, Siebels J, Cappato R and Kuck K-H 1996 Radiofrequency catheter ablation of left atrial tachycardia originating within the pulmonary vein in a patient with dextrocardia *Pacing Clin. Electrophysiol.* **19** 999–1002
Kallel F and Ophir J 1997 A least-squares strain estimator for elastography *Ultrason. Imaging* **19** 195–208
Lee W-N, Ingrassia C M, Fung-Kee-Fung S D, Costa K D, Holmes J W and Konofagou E E 2007 Theoretical quality assessment of myocardial elastography with *in vivo* validation *IEEE Trans. Ultrason. Ferroelectr. Freq. Control* **54** 2233–45
Lee W N, Provost J, Fujikura K, Wang J and Konofagou E E 2011 *In vivo* study of myocardial elastography under graded ischemia conditions *Phys. Med. Biol.* **56** 1155
Lesh M D *et al* 1994 Radiofrequency catheter ablation of atrial arrhythmias. Results and mechanisms *Circulation* **89** 1074–89
Lumens J *et al* 2015 Differentiating electromechanical from non-electrical substrates of mechanical discoordination to identify responders to cardiac resynchronization therapy *Circ. Cardiovasc. Imaging* **8** e003744

Luo J and Konofagou E E 2008 High-frame rate, full-view myocardial elastography with automated contour tracking in murine left ventricles *in vivo IEEE Trans. Ultrason. Ferroelectr. Freq. Control* **55** 240–8

Luo J and Konofagou E 2010 A fast normalized cross-correlation calculation method for motion estimation *IEEE Trans. Ultrason. Ferroelectr. Freq. Control* **57** 1347–57

Mozaffarian D *et al* 2015 Heart disease and stroke statistics—2015 update: a report from the American Heart Association *Circulation* **131** e29–322

Provost J, Gurev V, Trayanova N and Konofagou E E 2011a Mapping of cardiac electrical activation with electromechanical wave imaging: an *in silico–in vivo* reciprocity study *Heart Rhythm* **8** 752–9

Provost J, Lee W-N, Fujikura K and Konofagou E E 2010 Electromechanical wave imaging of normal and ischemic hearts *in vivo IEEE Trans. Med. Imaging* **29** 625–35

Provost J, Lee W-N, Fujikura K and Konofagou E E 2011b Imaging the electromechanical activity of the heart *in vivo Proc. Natl Acad. Sci.* **108** 8565–70

Provost J, Thiébaut S, Luo J and Konofagou E E 2012 Single-heartbeat electromechanical wave imaging with optimal strain estimation using temporally unequispaced acquisition sequences *Phys. Med. Biol.* **57** 1095–112

Provost J, Gambhir A, Vest J, Garan H and Konofagou E E 2013 A clinical feasibility study of atrial and ventricular electromechanical wave imaging *Heart Rhythm* **10** 856–62

Provost J *et al* 2011c Electromechanical wave imaging for arrhythmias *Phys. Med. Biol.* **56** L1–L11

Provost J *et al* 2015 Assessing the atrial electromechanical coupling during atrial focal tachycardia, flutter, and fibrillation using electromechanical wave imaging in humans *Comput. Biol. Med.* **65** 161–7

Ramanathan C, Ghanem R N, Jia P, Ryu K and Rudy Y 2004 Noninvasive electrocardiographic imaging for cardiac electrophysiology and arrhythmia *Nat. Med.* **10** 422–8

Richmond L *et al* 2008 Validation of computed tomography image integration into the EnSite NavX mapping system to perform catheter ablation of atrial fibrillation *J. Cardiovasc. Electrophysiol.* **19** 821–7

Sermesant M *et al* 2012 Patient-specific electromechanical models of the heart for the prediction of pacing acute effects in CRT: a preliminary clinical validation *Med. Image Anal.* **16** 201–15

Stevenson W G, Delacretaz E, Friedman P L and Ellison K E 1998 Identification and ablation of macroreentrant ventricular tachycardia with the CARTO electroanatomical mapping system *Pacing Clin. Electrophysiol.* **21** 1448–56

Szegedi N *et al* 2015 Radiofrequency ablation of focal atrial tachycardia: benefit of electroanatomical mapping over conventional mapping *Acta Physiol. Hung.* **102** 252–62

Tanner H *et al* 2010 Catheter ablation of recurrent scar-related ventricular tachycardia using electroanatomical mapping and irrigated ablation technology: results of the prospective multicenter Euro-VT-study *J. Cardiovasc. Electrophysiol.* **21** 47–53

Villarreal F J, Lew W Y, Waldman L K and Covell J W 1991 Transmural myocardial deformation in the ischemic canine left ventricle *Circ. Res.* **68** 368–81

Waldman L K, Fung Y C and Covell J W 1985 Transmural myocardial deformation in the canine left ventricle. Normal *in vivo* three-dimensional finite strains *Circ. Res.* **57** 152–63

Walker W F and Trahey G E 1994 A fundamental limit on the performance of correlation based phase correction and flow estimation techniques *IEEE Trans. Ultrason. Ferroelectr. Freq. Control* **41** 644–654

Yamane T *et al* 2001 Morphological characteristics of *P* waves during selective pulmonary vein pacing *J. Am. Coll. Cardiol.* **38** 1505–10